Trans Indian Inst Met (2017) 70(4):909–915
DOI 10.1007/s12666-016-0882-z

TECHNICAL PAPER

Influence of Carbon Equivalent Content on Phase Transformation During Inter-critical Heating of Dual Phase Steels Using Discrete Micro-scale Cellular Automata Model

K. Vijay Reddy[1] · C. Halder[2] · S. Pal[1]

Received: 19 December 2015 / Accepted: 28 March 2016 / Published online: 5 May 2016

Abstract In this paper, a cellular automata method based model is proposed for simulating phase transformation kinetics of inter-critical heating of dual phase (DP) steel. This developed model deals with the kinetics of pearlite dissolution, ferrite transformation and austenite grain growth based on carbon diffusion process. Diffusion equation is discretized and solved by finite difference method whereas austenite grain growth is controlled by transition rules applied in cellular automata algorithm. The model is operated in the temperature range of 730–890 °C for four different specimens of DP steel. This model predicts appropriately the microstructure and volume fraction of formed austenite during inter-critical heating of DP steel. In addition, this study shows that the presence of carbon and alloying elements enhances carbon equivalent of DP steel, helps in austenite formation.

Keywords Cellular automata · Dual phase steel · Inter-critical annealing · Carbon equivalent

1 Introduction

Dual phase (DP) steels are a classification of advanced high strength steels (AHSS) consisting of a hard martensitic phase in the matrix of ferrite along with retained austenite or bainite [1–3]. DP steels are basically low carbon low alloy steels produced through inter-critical annealing followed by quenching process [4]. DP steels are highly beneficial for aerospace and automotive industries as they possess low weight/strength ratio, high tensile properties, enhanced formability and ductility [5–8]. These favourable properties are related to the microstructure morphology of dual phase steel where soft ferritic phase enhances ductility and hard martensitic phase increases strength. The microstructure morphology is dependent on the inter-critical heat treatment temperature and process [9]. Distribution and volume fraction of martensite present in quenched DP steel is strongly influenced by volume fraction of transformed austenite and its dispersion during heating of DP steel [10]. Therefore, the austenite transformation during heating is significant in the development of the desired microstructure of DP steels although conventionally, much attention has been given to the transformation and the effect of alloying elements during cooling of austenite into ferrite [11–14]. Austenite transformation depends on grain size; grain distribution, concentration of alloying element, heating process and inter-critical annealing temperature [15]. Austenite stabilizers alloying elements (e.g. Ni, Mn, C) favours the transformation of austenite by decreasing the A_{c1} temperature whereas ferrite stabilizers (e.g. Cr, Mo) helps in the formation of ferrite by increasing the A_{c1} temperature [16, 17]. In addition, these alloying elements affect transformation rate, grain size, etc. during heating and also show significant impact on properties such as hardness, formability, and strength [17, 18]. Experimental investigations on the variation in microstructure and properties of DP steel produced by different heat treatment processes have been reported in literature [15, 19]. However, time constraints and research costs restrain the flexibility of conducting numerous and

✉ S. Pal
pals@nitrkl.ac.in

[1] Computational Materials Engineering Group, Metallurgical and Materials Engineering Department, National Institute of Technology Rourkela, Rourkela 769008, India

[2] Metallurgical and Materials Engineering Department, Indian Institute of Technology, Kharagpur 721302, India

rigorous experimental analysis. Numerical modelling as a consequence becomes an alternative and efficient tool for predicting the microstructure and properties by simulating the phase transformation process. However, conventional models based on Avrami type equations do not provide detail insight of mechanism related to the microstructure evaluation [20]. Hence to overcome this limitation, various logic/rule based mesoscale microstructure modelling tools such as cellular automata, phase field modelling have been applied. Many simulation models have been developed so far which have shown the kinetics of phase transformation during continuous as well as inter-critical annealing processes [21–23] and recrystallization [24, 25]. Since cellular automata (CA) can handle large computational domains and capable of reducing the code complexity in terms of storage therefore, CA modelling has advantages over phase field modelling [26]. A cellular automaton is a collection of grids or cells which have finite number of state variables in it. Evolution of microstructure can be predicted using cellular automata modelling by describing the discrete spatial and temporal variables and by applying deterministic or probabilistic transition rules [27–29]. Numerous CA modelling based prediction of microstructures for cooling part of transformation of DP steel are available in literature [24, 27, 29]. However, very few microstructure simulation studies using CA have been reported on austenite transformation during heating to inter-critical annealing temperature [30]. Moreover, the effect of alloying elements and carbon equivalent content has not been studied using the simulated models for the austenite transformation during inter-critical heating.

The objective of the present work is to develop a cellular automata model for predicting microstructure during the inter-critical heating of dual phase steel considering the phase transformation kinetics and study the effect of carbon equivalent on the austenite formation. The input microstructure in this model consists of ferrite and pearlite phases which are obtained from ferrite recrystallization model reported in literature [31]. Pearlite dissolution, ferrite transformation into austenite, and grain growth along with carbon diffusion is investigated in this paper. The developed model can be utilized as an initial microstructure for performing microstructure modelling for phase transformation during cooling.

2 Theoretical Background

Inter-critical annealing heat treatment of DP steel is performed on recrystallized specimen as recrystallization process causes grain refinement, redistributes the carbide and releases residual stress in the specimen [32]. The initial microstructure for inter-critical annealing consists of ferrite and pearlite grain. Hence, austenization process involves dissolution of pearlite grains and transformation of ferrite into austenite. The complete transformation process includes two major steps: austenite nucleation and growth [33]. Pearlite is a lamellar structure consisting of alternate layers of ferrite and cementite. The ferrite contains less than 0.025 wt% of carbon and cementite contains 6.67 wt% carbon. Steels with 0.77 wt% carbon contains uniform pearlite grains and directly transforms into austenite at eutectoid carbon concentration. Transformation of pearlite to austenite starts at A_{C1} temperature and nucleation of austenite occurs at ferrite/cementite interface inside pearlite. Due to short range of diffusion, the pearlite is transformed into austenite very rapidly containing a high concentration of carbon [34]. Once pearlite grains are transformed to austenite, the carbon is redistributed and ferrite transformation occurs. Ferrite is a low carbon concentration phase and the initial transformation into austenite is a slower process than pearlite dissolution. Pearlite to austenite transformation starts when the temperature is just above A_{C1}, the ferrite to austenite transformation is prominently observed at higher temperatures. Ferrite is transformed into austenite when the ferrite carbon concentration reaches the equilibrium carbon concentration (i.e. AB line) at that temperature as shown in Fig. 1. The equilibrium carbon concentration line and eutectoid composition (C_e) in Fig. 1 may change their position according to the composition of the steel. Steels with higher concentration of Mn, Ni, and Cu will lower the A_{C1} line; increase the A_{C3} lines and the eutectoid temperature thereby widening the temperature range over which austenite is stable whereas elements such as Si, Cr, Al, and P increase the A_{C1} temperature and the eutectoid temperature, thus restricting the formation of austenite [35].

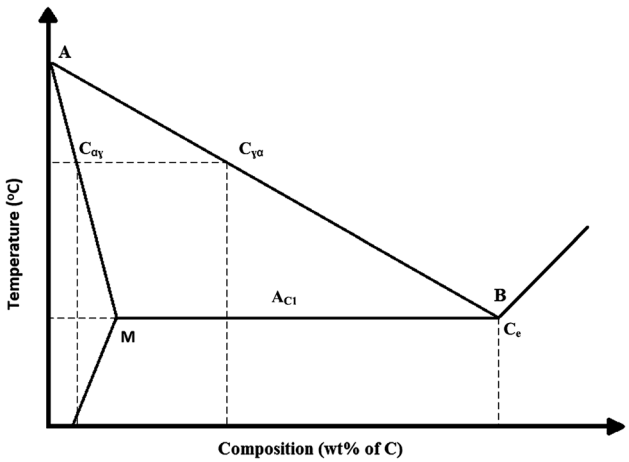

Fig. 1 Part of Fe-Fe_3C diagram

3 Development of Model

In the present model, cellular automata method is applied to simulate the phase transformation of ferrite-pearlite phase into austenite phase during heating in DP steel and predict the microstructure after inter-critical heating. In addition to that, the effect of equivalent carbon content of DP steel on austenite formation is investigated.

3.1 Dual Phase Steel Composition

In this paper, four different compositions of dual phase steel are considered and their compositions along with the carbon equivalent content are presented in Table 1. The volume fraction of ferrite and pearlite is calculated according to the weighted average of the carbon concentration of the DP steel specimen. The concentration of alloying element is varied to study their combined effect on the formation of austenite. The carbon equivalent (CE) content is calculated using Dearden and O'Neill equation [36]:

$$CE = C + \frac{P}{2} + \frac{Mn}{6} + \frac{Mo}{4} + \frac{(Cr + V)}{5} + \frac{Ni}{15} \quad (1)$$

where C, wt% of carbon concentration; P, wt% of phosphorous; Mn, wt% of manganese; Mo, wt% of molybdenum; Cr, wt% of chromium; V, wt% of vanadium; Ni, wt% of nickel in the steel.

3.2 Description of Model

The initial microstructure consists of pearlite grains in the matrix of ferrite. The spatial system is discretized into two dimensional cells. The dimension of each cell is 1 μm and the total domain consists of (147 × 495) cells. Each cell represents a set of variables—state variable and internal variable. State variables contain the information about the phase of the cell, internal variables contains information about carbon concentration and grain number. The kinetics of phase transformation is obtained by updating the variables according to the transition rules and heating rate. Two important transition rules are applied in this model for austenite nucleation and growth during the heating process.

3.3 Nucleation of Austenite Cells

In the present model the nucleation of austenite occurs at ferrite-pearlite interface. For nucleation, cells which are in ferrite phase and have pearlite cells in their Moore's neighbourhood are considered as nucleation site as per previously reported literature [30]. This restricts the nucleation cells only to the ferrite-pearlite interface. The favourable sites of nucleation are shown in Fig. 2. The pearlite is considered to be a uniform phase since the dimension of lamellar structure is in the order of 0.1 μm and the grains are in the order of 10 μm and this will increase the computational cost. However, to compensate the structural error, the concentration of pearlite cells is taken as the eutectoid concentration from the ThermoCalc diagrams shown in Fig. 3.

Nucleation occurs at a temperature above the A_{C1} line and the rate increases with increase in temperature. By literature, the number of austenite nuclei N is provided by the classical nucleation equation [37]:

$$N = \frac{1.378 \times 10^{-12}}{\left[(a^p)^2 \sigma_0\right]^2} \exp\left(\frac{-25.38}{T - A_{C1}}\right) \frac{1}{\text{mm}^3\,\text{s}} \quad (2)$$

where T is the temperature in degree Celsius, A_{C1} is the eutectoid temperature in degree Celsius and a^p, σ_0 are the morphological parameters for pearlite. But since this present model considers pearlite as a uniform phase, the nucleation equation may fail in determining the number of nuclei at different temperatures. To overcome this drawback, a probabilistic algorithm has been developed to determine the number of favourable nuclei that transforms into austenite. This algorithm counts the total number of favourable nucleation site present in the microstructure model. It then assigns a finite number of nucleation sites for each temperature. Depending on the heating rate, some of these assigned nuclei change their state to austenite. High heating rate results in more nucleation whereas slower heating rate results in less nucleation. Hence, by this process, the rate of nucleation changes as the temperature increases. Each cell which transforms into austenite nuclei takes a new state variable and a unique grain number but the carbon concentration is unchanged.

Table 1 Chemical composition of the specimens along with the carbon equivalent value

Specimens	C	Mn	Si	P	S	Cr	Mo	V	Al	Cu	Ni	Carbon equivalent
Specimen 1	0.13	1.5	0.10	0.011	0.011	0.23	0.005	0.005	0.026	0.02	0.02	0.318
Specimen 2	0.081	1.12	0.35	0.008	0.008	0.52	–	–	–	0.38	0.31	0.396
Specimen 3	0.11	0.53	0.07	0.02	0.02	0.03	–	–	–	–	0.03	0.216
Specimen 4	0.08	2.4	0.5	–	–	–	0.42	–	–	–	0.5	0.618

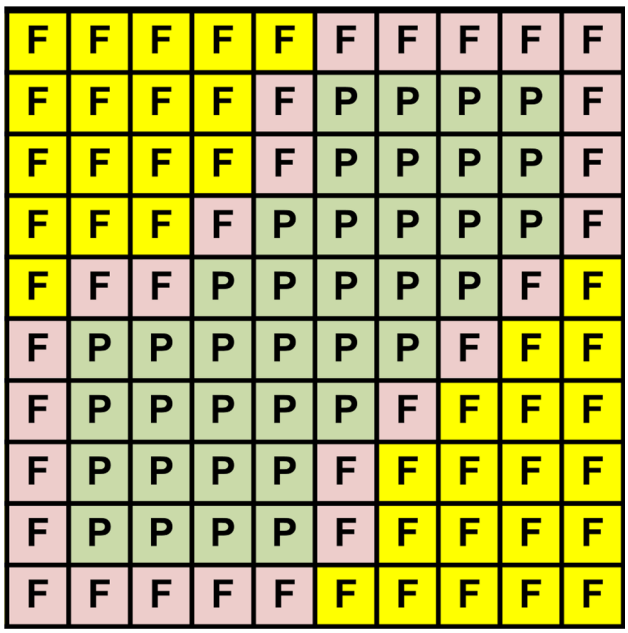

Fig. 2 Illustration of preferred nucleation sites (*cells with pink shade*) for austenite (*F* ferrirte, *P* pearlite)

3.4 Growth Process of Austenite

Austenite growth is controlled by the carbon diffusion process. To maintain a constant overall carbon concentration, periodic boundary conditions are applied in the model. Diffusion process is calculated by using discretized Fick's second law. Fick's second law is given by:

$$\frac{\partial C_\Psi}{\partial t} = D_\Psi \nabla^2 C_\Psi \tag{3}$$

where t is the time, C_Ψ is the concentration of solute, D_Ψ is the diffusion coefficient.

The discretized form is:

$$C_{i,j}^{t} = \frac{D_\Psi \Delta t}{\Delta_{xy}^2}\left(C_{i-1,j}^{t-1} + C_{i+1,j}^{t-1} + C_{i,j-1}^{t-1} + C_{i,j+1}^{t-1} + 4C_{i,j}^{t-1}\right) + C_{i,j}^{t-1} \tag{4}$$

where t is the time step, Δ_{xy} is dimension of one computational cell, i is the computational domain row and j is the computational domain column, $C_{i-1,j}^{t-1}$ is the cell on the left

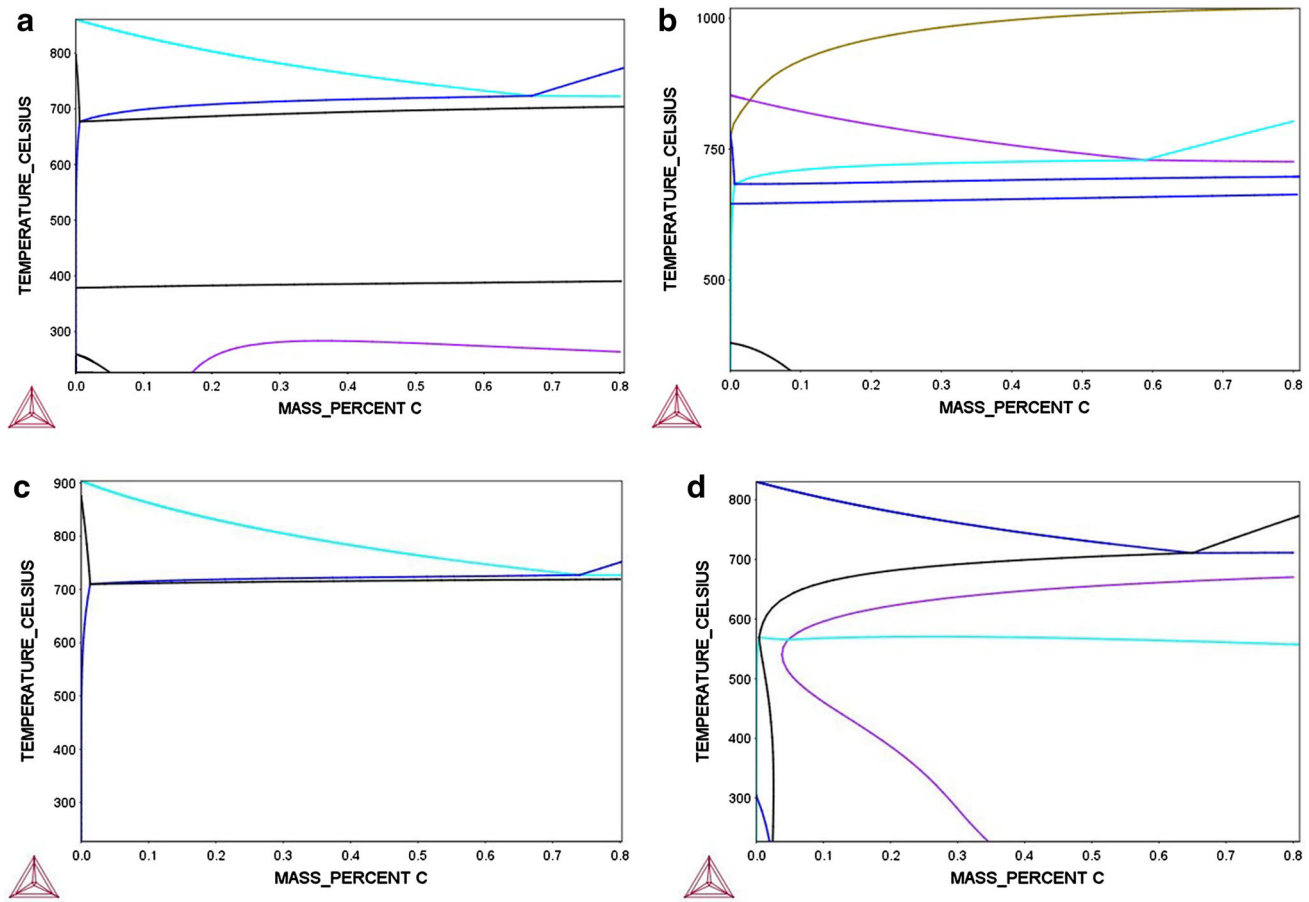

Fig. 3 ThermoCalc phase diagrams of dual phase steel of specimens: **a** → Specimen 1, **b** → Specimen 2, **c** → Specimen 3, **d** → Specimen 4

of the computed cell in the previous time step, $C_{i+1,j}^{t-1}$ is the cell on the right of the computed cell in the previous time step, $C_{i,j+1}^{t-1}$ is the cell above the computed cell in the previous time step, $C_{i,j}^{t-1}$ is the cell below the computed cell in the previous time step.

Δt is the condition of stability and is given by:

$$\Delta t \leq \frac{\Delta_{xy}^2}{4D\psi} \tag{5}$$

Diffusion coefficient for the carbon diffusion is calculated using the following equation:

$$D\psi = D_0 \exp\left(\frac{-Q_g}{RT}\right) \tag{6}$$

where D_0, 2.1×10^{-5} m^2 s^{-1} [21] is the pre exponential factor; Q_g, 141,500 J mol^{-1} [38] is the activation energy of migration; R, 8.314 J mol^{-1} K^{-1} is the gas constant, T is the absolute temperature in K.

The transition rules for the model are established in such a way that it shows the actual kinetics of transformation. The first transition rule is for the pearlite dissolution. The pearlite cell transforms into austenite as soon as the carbon concentration of the pearlite cell is reduced below the eutectoid temperature. The second transition rule is for the transformation of ferrite into austenite. The concentration of each cell is checked with the equilibrium carbon concentration after each time step. When carbon concentration of austenite cell exceeds the equilibrium carbon concentration at that temperature, then the neighbour ferrite cells transform into austenite.

To obtain realistic transformation kinetics, the equilibrium carbon concentration (A_{c3} line) curve is divided into line segments in different temperature ranges and linearly fit. The equilibrium carbon concentration is calculated by using Eq. 7. Table 2 provides the values for $C_{\gamma\alpha 0}^{A_{c3}}$ and $C_{\gamma\alpha 1}^{A_{c3}}$ at different temperature range for the specimens by linear curve fitting the equilibrium carbon concentration line obtained from ThermoCalc software.

$$C_{\gamma\alpha}^{A_{c3}} = C_{\gamma\alpha 0}^{A_{c3}} + C_{\gamma\alpha 1}^{A_{c3}} T \tag{7}$$

The temperature for the next time step is calculated according to the following equation:

$$T^{t+1} = T^t + \Delta t H \tag{8}$$

where H represents the heating rate and is equal to 3 °C s^{-1}, Δt is the time interval.

4 Results and Discussion

The representative initial microstructure and final transformed microstructure after simulated inter-critical heating up till 850 °C for specimen 1 are shown in Fig. 4a, b respectively. Final microstructure contains austenite grains, as all the pearlite and ferrite grains are transformed into austenite after the inter-critical heating. The microstructure evolution of austenite and the diffusion of carbon at different temperature during heating is presented in Fig. 5. The pearlite dissolution starts at 730 °C temperatures for all the specimens, which is evident from the representative microstructure of specimen 1 given in Fig. 5a. As the temperature increases, more and more pearlite is consumed for austenite transformation as per Fig. 5. The carbon diffusion increases with the increasing temperature and

Table 2 Values for $C_{\gamma\alpha 0}^{A_{c3}}$ and $C_{\gamma\alpha 1}^{A_{c3}}$ at different temperature range for the specimens by linear curve fitting the equilibrium carbon concentration line obtained from ThermoCalc software

Temperature range	Specimen 1	Specimen 2	Specimen 3	Specimen 4
730–740 °C				
$C_{\gamma\alpha 0}^{A_{c3}}$	6.0052	5.24362	5.53268	5.79362
$C_{\gamma\alpha 1}^{A_{c3}}$	−0.00736	−0.00646	−0.0.658	−0.00727
740–780 °C				
$C_{\gamma\alpha 0}^{A_{c3}}$	5.03996	4.38787	4.85085	4.62709
$C_{\gamma\alpha 1}^{A_{c3}}$	−0.00606	−0.0053	−0.00568	−0.00569
780–800 °C				
$C_{\gamma\alpha 0}^{A_{c3}}$	4.08956	3.77083	4.03145	3.77593
$C_{\gamma\alpha 1}^{A_{c3}}$	−0.00484	−0.0045	−0.00462	−0.0046
800–820 °C				
$C_{\gamma\alpha 0}^{A_{c3}}$	3.52916	3.23461	3.51962	3.1300
$C_{\gamma\alpha 1}^{A_{c3}}$	−0.00413	−0.00382	−0.00399	−0.00379
820–880 °C				
$C_{\gamma\alpha 0}^{A_{c3}}$	2.8849	2.67938	2.94599	3.00946
$C_{\gamma\alpha 1}^{A_{c3}}$	−0.00335	−0.00315	−0.00329	−0.00364

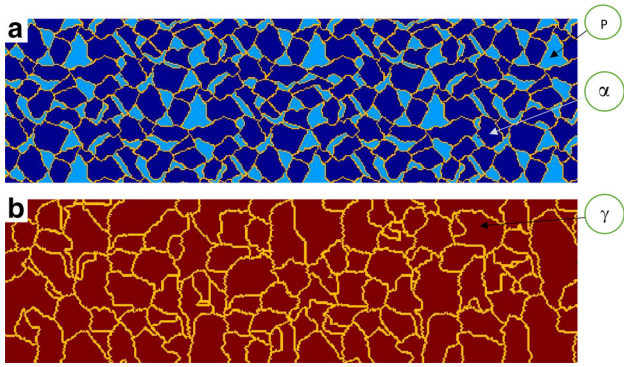

Fig. 4 **a** Initial microstructure as input for the simulation. **b** Final microstructure after transformation (P, pearlite; α, ferrite; γ, austenite)

consequently concentration of carbon in austenite reaches equilibrium state and the growth of austenite becomes steady. The complete austenite formation at 850 °C is evident in Fig. 5d.

The calculated austenite volume fraction and the experimental value obtained from literature [30] at different temperature for specimen is plotted in Fig. 6. The results obtained from the present simulation using CA method are found in a good agreement with the experiments.

It is obvious from Fig. 6 that the model can predict appropriately the austenite volume fraction after efficiently simulating the phase transformation kinetics for inter-critical heating of DP steel. Austenite volume fraction vs temperature for all four specimens is also plotted in separate figure to evaluate the effect of carbon equivalent on the volume fraction of austenite formed during inter-critical heating as shown in Fig. 7a. It is observed that transformation into austenite is completed at 890 °C for specimen 4 which has lowest carbon equivalent. On the other hand, austenite grows fastest and complete transformation occurs before 825 °C for specimen 3, which possess highest

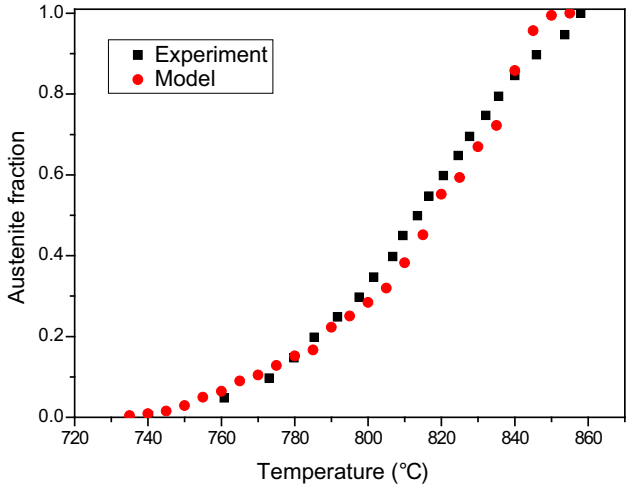

Fig. 6 Experimental vadiation of the simulated model for 3 °C s^{-1} heating rate

carbon equivalent content. The pearlite fractions at different temperature for all four specimens are presented in Fig. 7b. The complete pearlite dissolution is observed for all the specimens. In case of specimen having higher carbon equivalent, complete pearlite dissolution takes place at faster rate and lower temperature compared to the specimen having lower carbon equivalent. Therefore, it is inferred that the presence of carbon and alloying elements contributing in increment of carbon equivalent helps in faster formation of austenite.

5 Conclusion

A model for phase transformation during inter-critical heating of DP steel based on cellular automata method is designed and developed to predict microstructure and formation of austenite. The present study shows the capability

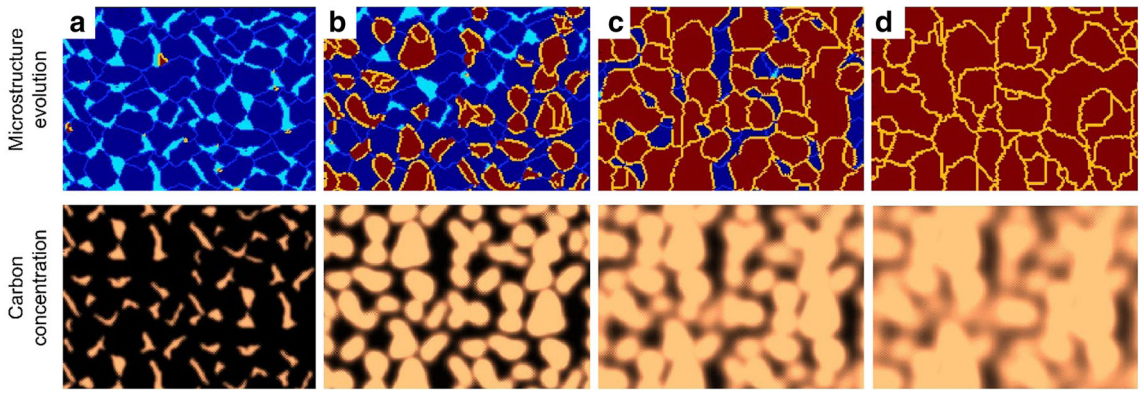

Fig. 5 Microstructure evolution along with carbon diffusion process during phase transformation at different temperatures: **a** 730 °C, **b** 770 °C, **c** 810 °C, **d** 850 °C

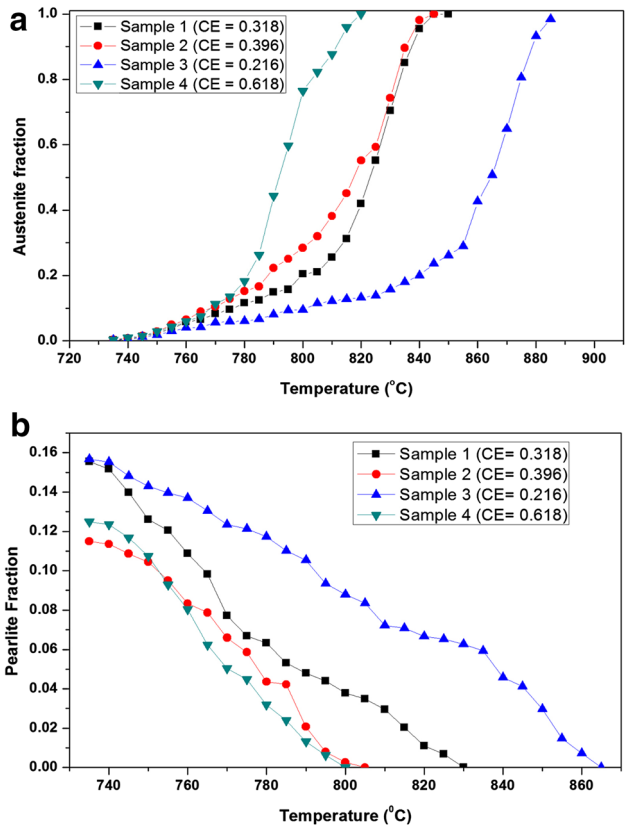

Fig. 7 Graph showing **a** the austenite fraction at different temperature for the specimens, **b** the pearlite fraction at different temperature for the specimens

of cellular automata based model for efficient simulation of phase transformation for DP steel. The model considers pearlite dissolution, ferrite transformation and austenite grain growth. This study shows that the carbon equivalent value is important for austenite transformation during intercritical heating of DP steels. Complete austenite transformation occurs faster for DP steels having higher carbon equivalent. The output of this predictive model is found to be in good agreement with literature reporting experimental results. This model can be extended and updated for identification and subsequent optimization of controlling parameters of phase transformation relevant to steel.

References

1. Al-Abbasi F M, and Nemes J A, *Int J Mech Sci* **45** (2003) 1449.
2. Rashid M S, *Annu Rev Mater Sci* **11** (1981) 1.
3. Sarwar M, and Priestner R, *J Mater Sci* **31** (1996) 2091.
4. Rocha R O, Melo T M F, Pereloma E V, and Santos D B, *Mater Sci Eng A* **391** (2005) 296.
5. Allam T, and Abbas M, *Steel Res Int* **86** (2015) 231.
6. Movahed P, Kolahgar S, Marashi S P H, Pouranvari M, and Parvin N, *Mater Sci Eng A* **518** (2009) 1.
7. Hofmann H, Mattissen D, and Schaumann T W, *Steel Res Int* **80** (2009) 22.
8. Matlock D K, Speer J G, De Moor E, and Gibbs P J, *Jestech* **15** (2012) 1.
9. Maleque M A, Poon Y M, and Masjuki H H, *J Mater Process Technol* **153** (2004) 482.
10. Erdogan M, *Scr Mater* **48** (2003) 501.
11. Zhang L, Zhang C B, Wang Y M, Wang S Q, and Ye H Q, *Acta Mater* **51** (2003) 5519.
12. Pandi R, and Yue S, *ISIJ Int* **34** (1994) 270.
13. Ricks R A, Southwick P D, and Howell P R, *J Microsc* **124** (1981) 23.
14. Cao J C, Liu Q Y, Yong Q L, and Sun X J, *J Iron Steel Res Int* **14** (2007) 52.
15. Huang J, Poole W J, and Militzer M, *Metall Mater Trans A* **35** (2004) 3363.
16. Schemmann L, Zaefferer S, Raabe D, Friedel F, and Mattissen D, *Acta Mater* **95** (2015) 386.
17. Girina O, Fonstein N, Panahi D, Bhattacharya D, and Jansto S, in *Microalloying 2015 & Offshore Engineering Steels 2015: Conference Proceedings (eds TMS),* Wiley, Hoboken (2015).
18. Speich G R, Demarest V A, and Miller R L, *Metall Trans A* **12** (1981) 1419.
19. Kim N J, and Thomas G, *Metall Trans A* **12** (1981) 483.
20. Todinov M T, *Acta Mater* **48** (2000) 4217.
21. Kulakov M, Poole W J, and Militzer M, *ISIJ Int* **54** (2014) 2627.
22. Pietrzyk M, Kuziak R, Radwański K, and Szeliga D, *Steel Res Int* **85** (2014) 99.
23. Zhu B, and Militzer M, *Metall Mater Trans A* **46** (2015) 1073.
24. Zhu G, Kang Y, Lu C, and Li S, *Steel Res Int* **85** (2014) 1035.
25. Bos C, Mecozzi M G, and Sietsma J, *Comput Mater Sci* **48** (2010) 692.
26. Pietrzyk M, Madej L, Rauch L, and Szeliga D, *Computational Materials Engineering: Achieving High Accuracy and Efficiency in Metals Processing Simulations*, Butterworth-Heinemann Newton, MA (2015).
27. Madej L, Sieradzki L, Sitko M, Perzynski K, Radwanski K, and Kuziak R, *Comput Mater Sci* **77** (2013) 172.
28. Han F, Tang B, Kou H, Cheng L, Li J, and Feng Y, *J Mater Sci* **49** (2014) 3253.
29. Mecozzi M G, Bos C, and Sietsma J, *Solid State Phenom* **172** (2011) 1140.
30. Halder C, Madej L, and Pietrzyk M, *Arch Civil Mech Eng* **14** (2014) 96.
31. Zheng C, and Raabe D, *Acta Mater* **61** (2013) 5504.
32. Ahmad E, Karim F, Saeed K, Manzoor T, and Zahid G H, in *IOP Conference Series: Materials Science and Engineering,* vol 60 (2014), p 012029.
33. Reed-Hill R E, Abbaschian R, Abbaschian L, *Phys Metall Princ* (2009) 4th edition, p 463.
34. Speich G R, Demarest V A, and Miller R L, *Metall Mater Trans A* **12** (1981) 1419.
35. Maalekian M, *Institut für Werkstoffkunde. Technische Universität Graz* **36** (2007). https://online.tugraz.at/tug_online/voe_main2.getvolltext?pCurrPk=32837.
36. Kasuya T, and Yurioka N, *Weld J* **72** (1993) 263.
37. Roosz A, Gacsi Z, and Fuchs E G, *Acta Mater* **31** (1983) 509.
38. Karacs G, and Roosz A, *Mater Sci Forum* **589** (2008) 317.